Competition of Crystalline and Liquid Crystalline Moieties in Self-Assembly of Poly(oxyethylene) Cholesterol Ethers

Jun-Ting Xu,* Liang Xue, and Zhi-Qiang Fan

Key Laboratory of Macromolecular Synthesis and Functionalization, Department of Polymer Science & Engineering, Zhejiang University, Hangzhou 310027, China

Zhong-Hua Wu

Beijing Synchrotron Radiation Laboratory, Institute of High Energy Physics, Chinese Academy of Sciences, Beijing 100039, China

Jin Kon Kim

National Creative Research Center for Block Copolymer Self-Assembly, Department of Chemical Engineering and Polymer Institute, Electronic and Computer Engineering Division, Pohang University of Science and Technology, Pohang, Kyungbuk 790-784, Korea

Received September 21, 2005; Revised Manuscript Received January 27, 2006

ABSTRACT: Self-assembly of a series of poly(oxyethylene) (POE) cholesterol ethers (ChEO*n*, $n = 5$, 10, 15, 20, 24, 30, and 45) bearing both liquid crystalline (LC) and crystalline moieties was studied by differential scanning calorimetry, wide-angle X-ray diffraction, Raman spectrometry, and small-angle X-ray scattering. In ChEO5 where POE is amorphous, the LC moiety was found to be dominant in determining morphology, and the repeating lamellar structure of ChEO5 is composed of double layers of cholesterol and a single layer of amorphous POE. In ChEO10 and ChEO15, LC and crystalline phases coexist and polymorphism is observed. The repeating lamellar structures of ChEO10 and ChEO15 are similar to that of ChEO5, except for the crystalline helical conformation of POE. With further increase in the chain length of POE, the crystalline POE becomes dominant in determining morphology, and the LC phase is not detected. The crystalline conformation of POE induces LC moieties to pack more closely, and the two LC layers gradually merge into a single LC layer in the repeating lamellar structure. Nonisothermal and isothermal crystallization experiments show that the preexisting LC phase can nucleate and accelerate POE crystallization, whereas the dimension of crystal growth of POE is reduced.

Introduction

Self-assembly of organic molecules into an ordered structure is usually driven by various driving forces, such as hydrogen bonding,[1] liquid crystalline,[2] crystallization,[3] microphase separation in block copolymers,[4] and so on.[5] When two or more driving forces are introduced into the same molecules, self-assembly becomes more complicated, and hierarchical structures at different scales may be formed.[6−21] Although the morphologies of some systems containing combined driving forces, for example, microphase separation/liquid crystalline[22−30] and microphase separation/crystallization,[15,31−33] have been well studied, the self-assembly driven by simultaneous crystallization and liquid crystalline has been seldom reported. Kunieda and others investigated the phase behavior of poly(oxyethylene) cholesterol ethers (ChEO*n*) with various lengths of poly(oxyethylene) (POE) in water[34−36] as well as the morphology of ChEO*n* in the bulk state.[37] Two different types of moieties exist in ChEO*n* (the cholesterol LC and POE moieties). They showed that for short chain length of POE (or $n \leq 15$) the LC phase of the cholesterol moiety and the POE crystalline phase coexist. But only the crystalline phase of the POE moiety was detected for ChEO*n* with $n > 15$. Then, they conclude by using small-angle X-ray scattering (SAXS) measurement that the conformation of POE in ChEO*n* with $n < 30$ was zigzag, whereas that in ChEO*n* with $n = 30$ was meandering.[37] However, some questions still need to be addressed. Since the degree of the competition between crystallization and LC depends on the chain length of POE moiety, the chain conformation of POE moiety should not be the same in all ChEO*n*s. In this paper, we demonstrate how the competition between the LC and crystalline moieties affects the packing of POE moiety and the superstructure of ChEO*n*s. We also investigate the effect of the preexisting LC phase on crystallization behavior of POE crystalline moiety. The present study would be helpful for controlling and regulating more precisely the self-assembly of amphiphilic molecules.

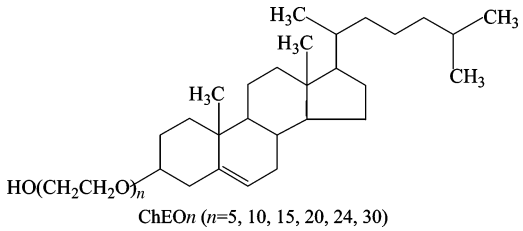

ChEO*n* (*n*=5, 10, 15, 20, 24, 30)

Figure 1. Chemical structure of poly(oxyethylene) cholesterol ethers.

Experimental Section

Materials. Poly(oxyethylene) cholesterol ethers, ChEO*n* (whose structure is shown in Figure 1 and *n* is the number of oxyethylene units, $n = 5$, 10, 15, 20, 24, and 30), were kindly donated by Japan Nihon Emulsion Co., Ltd. The samples were dried at 80 °C for 24 h and then stored at −18 °C. The polydispersity indexes of all the samples were measured by gel permeation chromatography (GPC) using tetrahydrofuran as a solvent. It was found that the polydispersity indices of ChEO*n* with $n \geq 15$ are 1.11, but those for ChEO5

* Corresponding author: e-mail xujt@zju.edu.cn; Fax 0086-571-87952400.

10.1021/ma052051s CCC: $33.50
Published on Web 03/25/2006

and ChEO10 are 1.20 and 1.22, respectively. The chemical structure and the weight fraction of POE moiety in ChEO*n*s were verified by ^{1}H NMR (Bruker AMX500 NMR spectrometer). The GPC traces and NMR spectra of all ChEO*n* are given in the Supporting Information. ChEO45 was prepared by coupling of cholesterol and poly(ethylene glycol) monomethyl ether ($M_n = 2000$, $M_w/M_n = 1.06$) using terephthaloyl chloride (TPC) as coupling reagent. 4.0 g of poly(ethylene glycol) monomethyl ether was dissolved in 60 mL of chloroform, and 4.03 g of TPC was dissolved in 30 mL of dry chloroform. The PEG monomethyl ether/chloroform solution was slowly dropped into a TPC/chloroform solution. The resulting solution was stirred under nitrogen at 65 °C for 24 h. Chloroform was removed under vacuum, and the excessive TPC in the solid was washed by diethyl ether for at least five times under nitrogen. The residue was dried by vacuum and dissolved in 60 mL of chloroform. This solution was slowly dropped into another chloroform solution containing cholesterol (5 g in 20 mL) and stirred under nitrogen at 65 °C for 24 h. The solution was cooled to room temperature and washed by diethyl ether, and a white solid precipitated. The solid was dried in a vacuum at room temperature for 24 h. The product was characterized with ^{1}H NMR.

Differential Scanning Calorimetry (DSC). DSC experiments were carried out on a TA Q100 instrument. The samples were first held at 160 °C for 5 min to erase thermal history, then cooled to −50 °C at a rate of 10 °C/min, and again heated to 160 °C at a rate of 10 °C/min. To investigate the effect of LC phase on crystallization of POE moiety, the samples were cooled from 160 to 20 °C at two different cooling rates, 100 and 10 °C/min; then the samples were cooled from 20 to −50 °C at a constant rate of 10 °C/min. Finally, the samples were also heated to 160 °C at a rate of 10 °C/min.

For isothermal crystallization experiments for ChEO10, the sample was directly cooled from 160 °C to a crystallization temperature ($T_c = -14$ °C) at a rate of 100 °C/min. To facilitate the formation of LC phase, the sample was first cooled to 20 °C at a rate of 10 °C/min and held at 20 °C for 5 min and then cooled to the same crystallization temperature ($T_c = -14$ °C) at a rate of 100 °C/min. The change of heat flow with time was recorded upon crystallization. The isothermal crystallization kinetics of polymer was analyzed by using the Avrami equation:[38]

$$1 - X(t) = \frac{\Delta H^c_{t=\infty} - \Delta H^c_t}{\Delta H^c_{t=\infty} - \Delta H^c_{t=0}} = \exp(-kt^m) \quad (1)$$

where $X(t)$ is the relative crystallinity at time t; $\Delta H^c_{t=\infty}$ and ΔH^c_t are the enthalpies at complete crystallization and at time t, respectively. The crystallization rate constant k and Avrami exponent m can be determined from the intercept and slope in the plot of $\ln[-\ln(1 - X(t))]$ vs $\ln(t)$.

$$\ln[-\ln(1 - X(t))] = \ln k + m \ln t \quad (2)$$

Wide-Angle X-ray Diffraction (WAXD) and Small-Angle X-ray Scattering (SAXS). WAXD experiments were carried out on a Rigaku D/max 2550PC diffractometer (40 kV, 300 mA) using Ni-filtered Cu Kα radiation in a step of 0.02° from 3° to 60°. Synchrotron SAXS measurements were performed at beamline 4B9A at the Beijing Synchrotron Radiation Facility,[39] with q ranges of 0.005 Å^{-1} < q < 0.15 Å^{-1}, where $q = 4\pi \sin(\theta/2)/\lambda$, with θ and λ being respectively the scattering angle and incident X-ray wavelength of 1.54 Å. The exposure time was ∼5 min for each sample. The distance between the sample and the detector was 1.52 m. Scattering profiles of the samples were obtained by an image plate (Mar345) detector and analyzed with a Fit2D program.

Atomic Force Microscopy (AFM). The thin film morphology of ChEO10 and ChEO15 was investigated by atomic force microscopy (SPA 300HV/SPI3800N Probe Station, Seiko Instruments Inc., Japan) in tapping mode with a silicon microcantilever (spring constant 16 N/m and resonance frequency ∼138 kHz). The scan rate ranged from 0.5 to 2.0 Hz to optimize the quality of AFM image. The set-point ratio, the ratio between the set-point amplitude and the free vibration amplitude (the lowest amplitude when tip and sample are not in contact), was chosen to be ∼0.8. Thin films were prepared by spin-coating from dichloromethane solution of ChEO10 and ChEO15 (1.0% w/v)on a clean mica. After complete removal of the solvent, the thin films were stored at −18 °C for 2 days to complete crystallization. The thickness of the lamellar structures was obtained directly from the cross-sectional profiles.

Raman Spectroscopy. Raman spectra were recorded on a Nicolet Almega XR dispersive Raman spectrometer equipped with an Olympus BX50 microscope. Measurements were operated at a laser wavelength of 785 nm, and the laser irradiation spot size was about 10 μm. Before experiments, the samples were stored at −18 °C for 2 days to complete crystallization.

Polarized Optical Microscopy (POM). POM experiments were conducted at room temperature on an Olympus BX-51 polarized optical microscope equipped with a digital camera. A small amount of samples was placed on a glass slide and covered with a thin glass slide. The thickness of samples was about 10 μm. The treatment of samples was the same as that in Raman experiments.

Results and Discussion

Structure of ChEO*n*. Figure 2a,b shows the cooling and heating DSC traces of ChEO*n*. For ChEO5, only the liquid crystal/isotropic transition of the cholesterol unit was observed. The crystallization (or melting) peak of POE was not detected due to the presence of the LC unit, though neat POE with $n = 5$ can be crystallizable at a lower temperature. The melting temperature of neat POE with $n = 5$ was reported to be 9 °C.[40] On the other hand, for ChEO*n* with $n = 20$, 24, 30, and 45, only the crystallization (or melting) peak of POE was observed. Interestingly, for $n = 10$ and 15, both crystallization (or melting) transition from POE moiety and LC/isotropic transition from LC moiety were seen. These findings are similar to those reported previously.[37] It is seen from Figure 2 that with an increase in the chain length of POE the LC/isotropic transition temperature decreases gradually, while the melting (or crystallization) temperature of the POE moiety increases.

Figure 3 shows the WAXD patterns of ChEO*n* measured at 25 °C after crystallization at −18 °C for 2 days. Except for ChEO5, all ChEO*n*s exhibit two crystalline peaks appearing at $2\theta = 19.0°$ and 23.0°, corresponding to (120) and (112 + 032) reflections of monoclinic POE crystals, respectively. This shows that the crystal structure of POE in ChEO*n* is similar to that of high molecular weight POE homopolymer. Crystallinity of POE in ChEO*n*s increases dramatically with increasing the chain length of POE. But, ChEO5 exhibits two broad peaks: one appearing at $2\theta \sim 16°$ due to cholesterol LC moiety and the other appearing at $2\theta \sim 23°$ due to amorphous (*not crystalline*) POE. To confirm these arguments, the ChEO*n* samples were first melted at 160 °C and then quenched to 25 °C at a rate of 100 °C/min. Under this cooling condition, the POE moiety in all ChEO*n*s except ChEO30 and ChEO45 cannot crystallize at 25 °C (see Figure 2a). Figure 4 gives WAXD profiles of all ChEO*n*s measured at 25 °C after quenching from 160 °C. Two amorphous peaks were clearly seen for three samples (ChEO5, ChEO10, and ChEO15). The ratio of the peak intensity at $2\theta \sim 16°$ to that at $2\theta \sim 23°$ decreases gradually with increasing n. Also, the peak at $2\theta \sim 16°$ disappears for n greater than 20. This is in accordance with the DSC result given in Figure 1 that LC/isotropic transition was not observed for these samples. The distance ($d = \lambda/(2 \sin \theta^*)$ in which θ^* is the diffraction angle at the peak intensity) between two cholesterol LC moieties and the distances between (120) and (112) reflections of POE crystals are shown in Figure 5. It is found that the distance between two cholesterol moieties decreases rapidly with in-

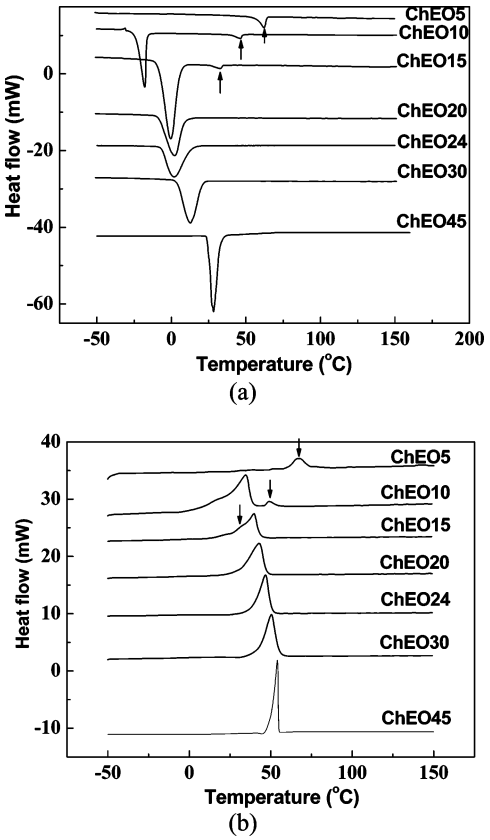

Figure 2. DSC traces of ChEO*n*s (a) during cooling run from 160 to −50 °C at rate of 10 °C/min and (b) heating run from −50 to 160 °C at rate of 10 °C/min. The isotropic/LC transition is indicated by the arrow.

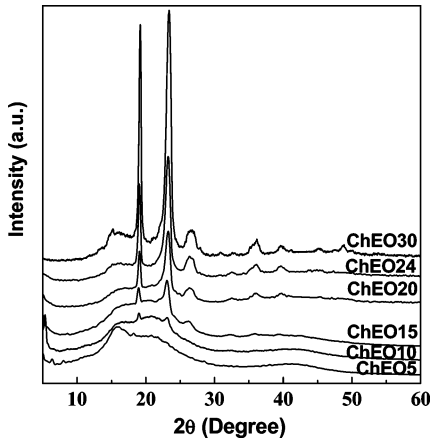

Figure 3. WAXD patterns of ChEO*n*s measured at 25 °C after crystallization at −18 °C for 2 days.

creasing *n*, whereas the *d*-spacing of (120) and (112) reflections maintain nearly constant irrespective of *n*. This shows that crystallization of POE moiety could induce more dense packing of cholesterol LC moiety.

Figure 6 shows Raman spectra of ChEO*n*s measured at 25 °C after crystallization at −18 °C for 2 days. The peaks at 1441 and 1481 cm^{-1} correspond to CH_2 bending mode for amorphous POE with TGG and TGT conformations (T and G designate trans and gauche conformations, respectively) and the monoclinic structure of crystalline POE with TGT conformation, respectively.[41] For ChEO5, the peak at 1481 cm^{-1} is barely seen, indicating that POE moiety in ChEO5 could not form crystalline structure. With increasing *n*, the relative intensity ratio of the peak at 1481 cm^{-1} to that at 1441 cm^{-1} increases gradually,

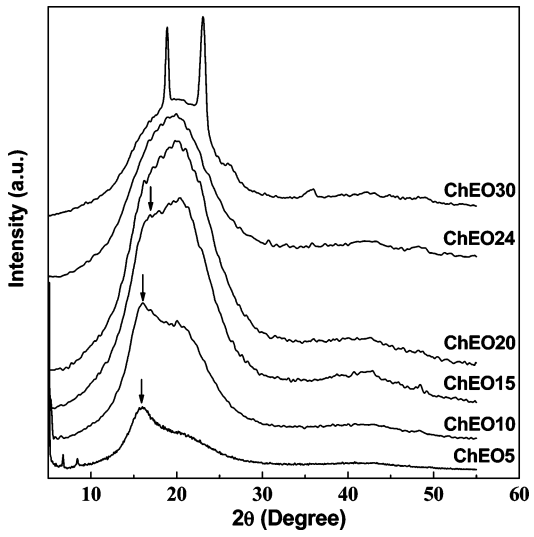

Figure 4. WAXD patterns of ChEO*n*s measured at 25 °C after quenching from molten state (160 °C). ChEO30 crystallizes at this temperature. The arrows indicate the peaks from LC phase.

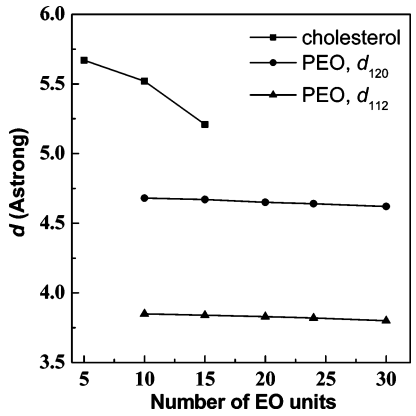

Figure 5. Change of the distance between two cholesterol units and the *d*-spacings of (120) and (112) reflections of POE crystals with the chain length of POE.

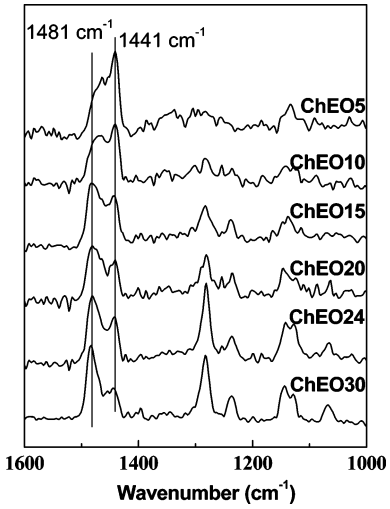

Figure 6. Raman spectra of ChEO*n*s measured at 25 °C after crystallization at −18 °C for 2 days.

suggesting that POE crystallinity increases, which is in accordance with WAXD results.

Figure 7 shows the SAXS profiles of ChEO*n*s at 25 °C after crystallization at −18 °C for 2 days. The peak positions show that lamellar structure is formed for all samples. However, only

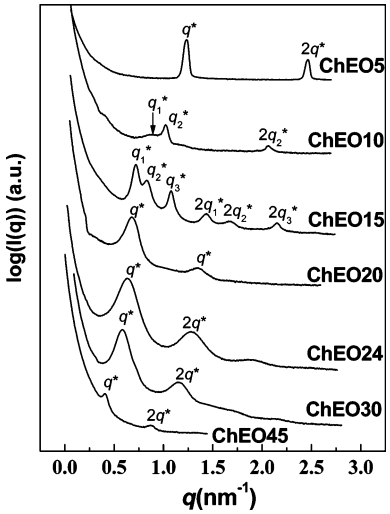

Figure 7. SAXS profiles of ChEO*n*s measured at 25 °C after crystallization at −18 °C for 2 days. The q^* and $2q^*$ indicate the first- and second-order SAXS peaks of a lamellar structure. q_1^*, q_2^*, and q_3^* represent the first-order peaks of different lamellar structures.

one type of lamellar structure is observed for ChEO5, ChEO20, ChEO24, ChEO30, and ChEO45, whereas more than two kinds of lamellar structure are present in ChEO10 and ChEO15. Notice that ChEO10 and ChEO15 exhibited coexistence of crystalline and LC phases, as evident from DSC and WAXD results. Different types of lamellar structures seen in ChEO10 and ChEO15 were confirmed from AFM images given in Figure 8. Lamellar structure was observed for these two samples (Figure 8a,c). The existence of other structures (such as hexagonal or sphere structure) can be excluded to a large extent. Since mica strongly absorbs the POE unit and the hydrophobic cholesterol units tends to locate at the polymer/air interface, the pattern should have been observed by AFM, if there exist other structures. However, we find that the lamellar thickness is not uniform, as shown in the cross-sectional height AFM profiles (Figure 8b,d). This suggests that ChEO10 has indeed two lamellar structures with two different lamellar thicknesses of 6.1 and 6.8 nm, which are very close to the values (6.1 and 7.1 nm) determined from SAXS. On the other hand, ChEO15 has three lamellar structures with thicknesses of 5.8, 7.3, and 8.5 nm which are similar to those determined from SAXS. The above conclusion based on the SAXS profiles is not consistent with the result given by Kunieda et al.,[37] even if the results of DSC and WAXD in this study are essentially the same as those in ref 37. We consider that this difference might be due to the fact that these two samples in ref 37 were not fully crystallized at low temperature prior to SAXS experiment. The other possibility is that we employed synchrotron SAXS, which is much more powerful in detecting small change of morphology compared with conventional SAXS employed in ref 37.

To explain the lamellar structure in all samples, three possible packing models are considered for an amphiphilic molecule composed of both rigid and flexible units,[42] as shown in Figure 9. The repeating structure contains two layers of rigid units and

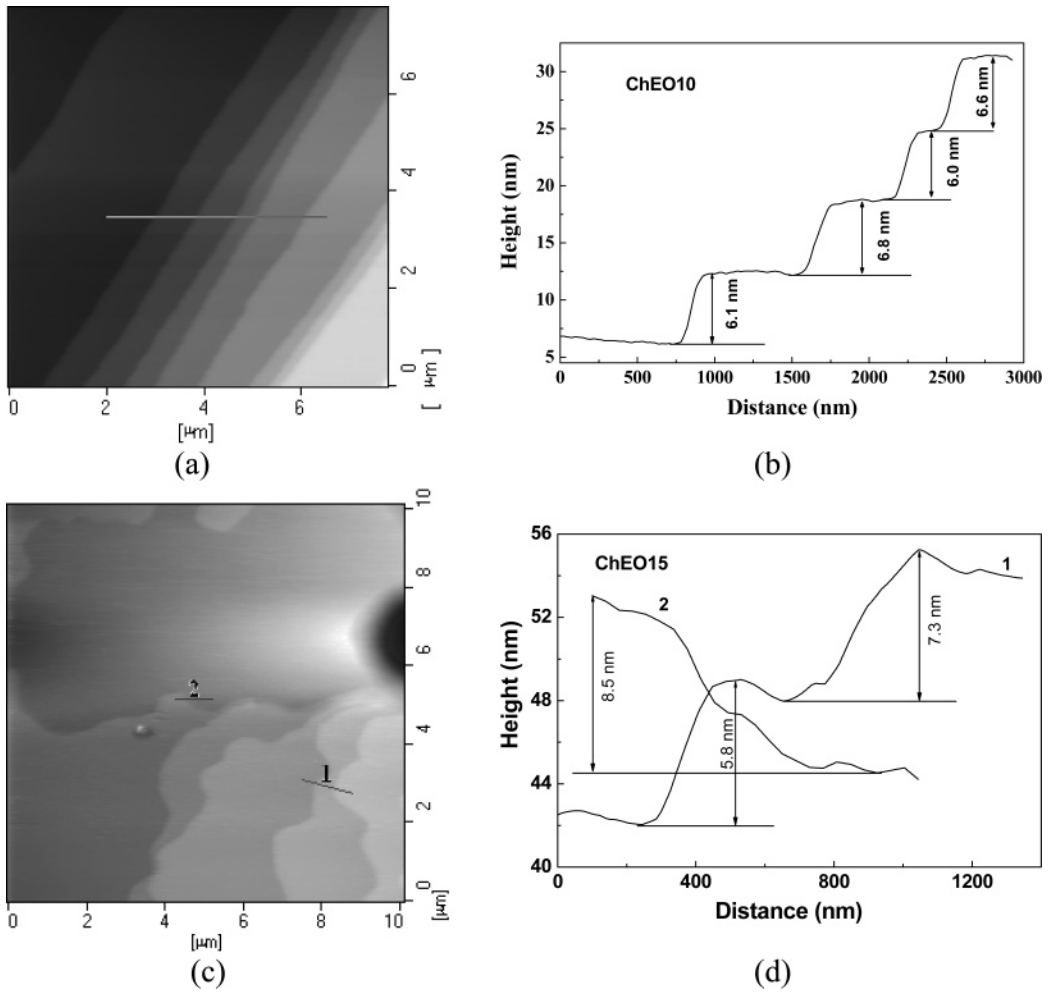

Figure 8. AFM height images (a and c) and cross-sectional height profiles (b and d) of ChEO10 and ChEO15 thin film prepared by spin-coated onto a clean mica: (a) and (c) for ChEO10; (b) and (d) for ChEO15.

Table 1. Experimental and Calculated Long Periods of Poly(oxyethylene) Cholesterol Ethers after Crystallization

		calculated L (Å)[a]						
n	experimental L (Å)	$2a + nb$	$2a + nb'$	$a + nb$	$a + nb'$	$2a + 2nb$	$2a + 2nb'$	possible structures[b]
5	50.8	50.0		30.0		60.0		I
10	71.5, 61.5	60.0	68.5	40.0	48.5	80.0	97.0	I, II
15	87.1, 75.5, 58.3	70.0	82.8	50.0	62.8	100.0	125.6	II, III, IV[c]
20	92.9		97.0		77.0		154.0	III
24	98.7		108.4		88.4		176.8	III
30	108.1		125.5		105.5		210.0	IV
45	154.6		168.3[d]		148.3[d]		296.6	IV

[a] The size of hydroxyl end group is not included. [b] Corresponding to the structures in Figure 10. [c] The conformation of poly(oxyethylene) moiety is not fully helical. [d] The size of terephthaloyl from coupling reagent is not included.

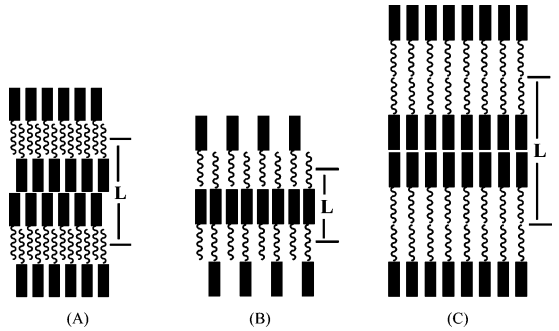

Figure 9. Three possible packing models for an amphiphilic molecule with both rigid and flexible units.

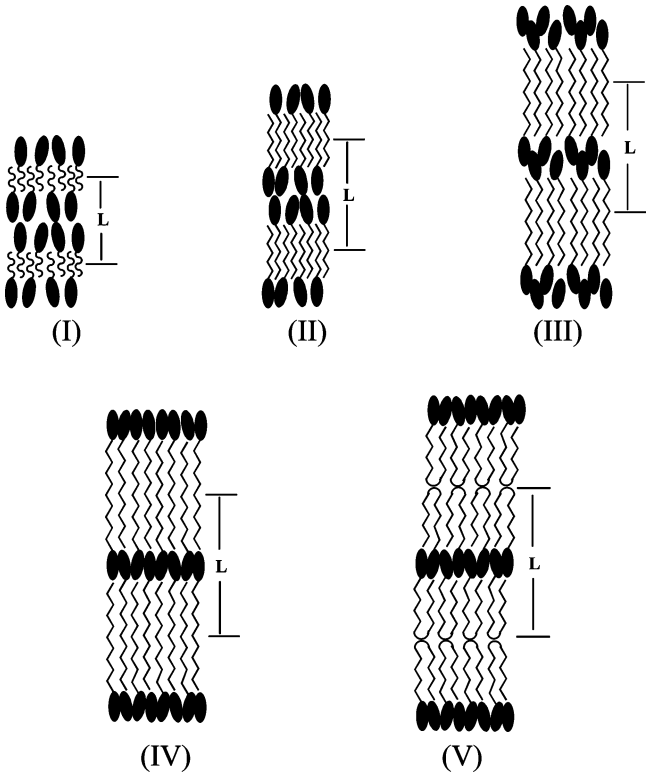

Figure 10. Schematic of different lamellar structures for ChEO*n*s.

one layer of flexible unit for model A, but it consists of a single rigid layer and single flexible layer for model B. Finally, it is composed of two layers of rigid units and two layers of flexible units for model C. In these models, we do not consider chain tilting effect. When the cross-sectional areas of the rigid and the flexible units mismatch and the rigid unit occupies larger cross-sectional area, chain tilting occurs to gain larger cross-sectional area for the flexible chain. In monoclinic POE crystals, the cross-sectional area per POE chain is about 21 Å^2,[43] while the cross-sectional area per cholesterol molecule is calculated to be 5.5 Å $\times$ 4.2 Å $=$ 23 Å^2 by using the software of "ChemOffice" (see the Supporting Information), which is slightly larger than that of POE chain. However, since one cholesterol molecule is not symmetric at both ends, antiparallel packing of two cholesterol molecules will lead to a smaller cross-sectional area. Therefore, we consider that the cross-sectional area occupied by the LC moiety in ChEO*n*s would be similar to that of the crystalline moiety, and thus chain tilting does not happen. For ChEO*n*s with amorphous POE chains, the cross-sectional area per POE chain is larger than that in crystalline state due to loose packing, and there is no need of chain tilting either.

In ChEO*n*s the POE chains may exhibit different conformations, varying with POE chain length. The amorphous POE moiety adopts a meander conformation with the size of one EO unit (b) of about 2 Å,[44] while monoclinic PEO crystals take helical conformation with one EO unit (b') of about 2.85 Å.[45] The size (a) of extended cholesterol moiety was about 20.0 Å.[46] Then, the long periods are $L = 2a + nb$ (or $L = 2a + nb'$) for model A, $L = a + nb$ (or $L = a + nb'$) for model B, and $L = 2a + 2nb$ (or $L = 2a + 2nb'$) for model C. From WAXD results, the POE in ChEO5 becomes amorphous; thus, only the meander conformation is considered. Also, only the helical conformation is used for POE in ChEO20, ChEO24, ChEO30, and ChEO45. But both amorphous and helical conformations are used for ChEO10 and ChEO15. Experimentally obtained L by SAXS and the calculated L based on three models for the crystallized ChEO*n* are summarized in Table 1, where the calculated L on the basis of model C is distinctly larger than the measured L. Thus, model C is not valid for all samples.

Based on Table 1, the lamellar structures of all samples are schematically given in Figure 10. The lamellar structure of ChEO5 contains two layers of LC moiety and one layer of amorphous POE (structure I). In ChEO10, there are two types of lamellar structure, and both are in accordance with model A. The difference in these two lies in the conformation of POE: amorphous (structure I) and crystalline (structure II). Three types of lamellar structures are identified in ChEO15 from SAXS. The largest lamellar structure with $L = 87.1$ Å is composed of two layers of LC moiety and one layer of crystalline POE (structure II). The smallest long period ($L =$ 58.3 Å) suggests that the lamellar structure might result from model B with different conformations (structure IV), suggesting that the POE is partially crystallized. The middle value of the long period ($L = 75.5$ Å) corresponds to the lamellar structures based on either model A or model B with crystalline conformation (structure III). ChEO20 and ChEO24 also have lamellar structure III.

For ChEO30 and ChEO45, the calculated L from model B in Figure 9 are very close to the experimental values, showing that the lamellar structure in these two samples contains only a

single layer of cholesterol moiety and a single layer of crystalline POE (structure IV). But another possible structure might exist for ChEO30 and ChEO45 that contains double layers of once-folded POE moiety and one layer of cholesterol (structure V). This structure has the same long period as structure IV. However, this possibility is excluded because the calculated melting temperatures of once-folded POE moiety in ChEO30 and ChEO45 are 35.1 and 45.5 °C, respectively,[47] which are distinctly lower than the observed values (50.4 °C for ChEO30 and 54.0 °C for ChEO45). Based on results given in Table 1 and Figures 9 and 10, the morphology changes from one lamellar structure composed of double layers of cholesterol units and a single layer of amorphous POE unit into another consisting of double layers of cholesterol units and a single layer of crystalline POE unit; then the double cholesterol layers are gradually merged into a single layer, with increasing *n*. The merging of a double layer of cholesterol units into a single layer is very interesting, and this phenomenon has not been reported in the literature. The reason can be explained on the basis of the change of POE chain conformation with different *n*. Namely, POE chains become more extended and closely packed with increasing *n*. In this situation, the interfacial area occupied by one cholesterol unit is reduced, which induces more close packing of cholesterol units by decreasing the distance between two cholesterol units (Figure 5).

The packing structures of ChEO*n*s based on SAXS data are not consistent with those proposed by Kunieda et al.[37] They proposed that in all ChEO*n*s except ChEO30 the repeating structure contains a single layer of POE chains and double layers of cholesterol molecules, in which the POE chains are antiparallel packed with a zigzag conformation and totally overlapped, while in ChEO30 the POE chains take a meander conformation and are partially overlapped. However, this model contradicts the observed DSC and WAXS results that the POE in ChEO5 is amorphous but is crystallizable in other ChEO*n*s. Finally, we consider the detail of polymorphism observed for ChEO10 and ChEO15. One might consider that partial melting of POE crystals in ChEO10 and ChEO15 at the SAXS measurement temperature, which can be judged from DSC results, leads to the existence of polymorphism. But partial melting cannot play a major role in the formation of polymorphism in ChEO10 and ChEO15 because the crystallinity of POE becomes quite low in ChEO10 and ChEO15, indicating that most of POE chains remain amorphous in both samples, even though these two samples were cooled to a low temperature. On the basis of the morphological development of ChEO*n*s with *n* and the fact that LC and crystalline phases coexist in ChEO10 and ChEO15, we consider that the existence of polymorphism in both samples is due to the fact that LC moiety and crystalline POE moiety have a similar effect on the final morphology. Namely, neither LC moiety nor crystalline moiety prevails over the other to affect the final morphology. Another issue that should be addressed is whether the LC phase and crystalline phase can be accommodated in the same lamellar layer. The SAXS results show that ChEO10 has two lamellar structures. By comparing the experimental *L* and calculated *L* from various models, we know that POE adopts amorphous and crystalline conformation in these two structures, respectively. It is possible that the LC phase observed in ChEO10 is located at the lamellar structure containing amorphous POE, or the LC phase coexists with crystalline POE in the same structure. For ChEO15 having three types of lamellar structures as evident from SAXS results (Figure 7), the conformation of the POE moiety is not completely amorphous even at the smallest $L = 58.3$ Å. Thus, we consider that the LC phase and POE crystalline phase coexist in the same lamellar structure for ChEO15.

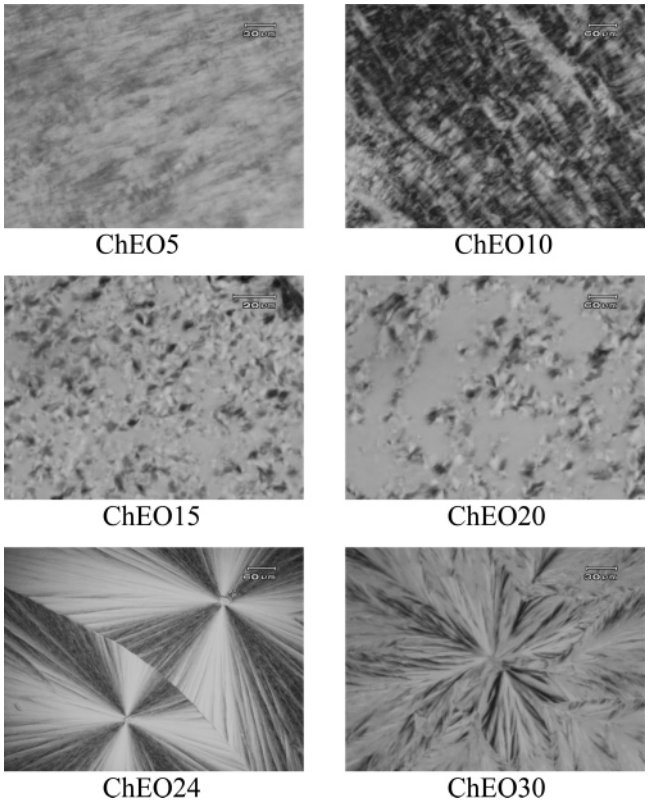

Figure 11. POM micrographs of ChEO*n*s measured at 25 °C after crystallization at −18 °C for 2 days.

Morphology of ChEO*n*. The competition of LC and crystalline moieties affects not only the packing model but also the superstructures of ChEO*n*s. Figure 11 shows the POM micrographs of ChEO*n*s measured at 25 °C after crystallization at −14 °C for 2 days. ChEO5 and ChEO10 exhibit LC morphology with band structure. This indicates that the cholesterol LC unit is dominant in determining the final morphology for these two samples, although POE in ChEO10 is crystallizable. Tiny and imperfect spherulites are observed in ChEO15 and ChEO20, showing that the crystalline POE unit already overwhelms the LC unit in deciding the final morphology for these two samples. With further increase in the length of POE, ChEO24 and ChEO30 form large and perfect spherulites, and the LC unit has little effect on the superstructure of POE.

Effect of Preexisting LC Phase on Crystallization of POE Moiety. In ChEO10 and ChEO15, the LC phase and crystalline phase coexist. Since the LC phase is formed prior to the crystalline phase during cooling, the preexisting LC phase may influence the crystallization of POE moiety. To investigate this effect, ChEO10 and ChEO15 were cooled from 160 to 20 °C at two different cooling rates: 100 and 10 °C/min. The higher cooling rate retards the formation of LC phase, and the slower cooling rate was used to develop a well-defined LC phase. Subsequently, these two samples were cooled from 20 to −50 °C at the same rate of 10 °C/min to complete the crystallization of POE moiety. After crystallization the samples were heated to molten state at a rate of 10 °C/min. Figure 12 illustrates DSC traces of ChEO10 and ChEO15 during cooling, and Figure 13 shows DSC traces of ChEO10 during heating. The DSC traces of ChEO15 during cooling are not shown because the LC−isotropic transition and melting temperatures overlapped. It can be seen from Figure 13 that the melting enthalpy of LC phase

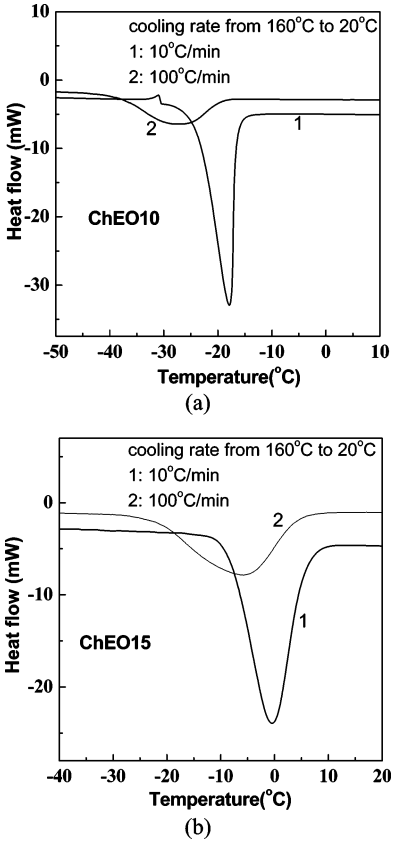

Figure 12. DSC traces of (a) ChEO10 and (b) ChEO15 during cooling run from 20 to −50 °C at a rate of 10 °C/min after experiencing cooling history from 160 to 20 °C at two different cooling rates (10 °C/min for curve 1 and 100 °C/min for curve 2).

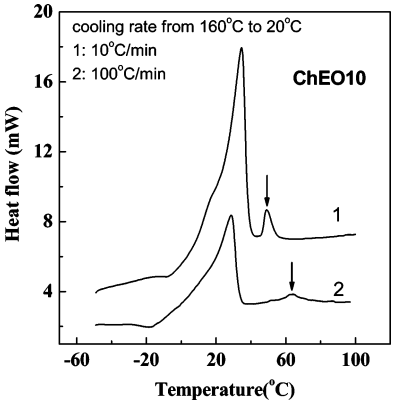

Figure 13. DSC traces of ChEO10 during heating run from −50 to 100 °C at a rate of 10 °C/min after crystallization at different conditions described in Figure 11. The arrows indicate the LC/isotropic transition.

of a sample experiencing cooling history at a cooling rate of 10 °C/min is much larger than that at a cooling rate of 100 °C/min, indicating a more perfect LC phase is developed. Comparing the DSC curves of POE moiety at different cooling rates (Figure 12), a more perfect preexisting LC phase leads to higher crystallization temperature and faster crystallization rate (reflected by the sharper crystallization peaks). These findings show that a preexisting LC phase affects nucleation during crystallization of POE moiety and accelerates crystallization of POE, which is very similar to blends consisting of crystalline polymer/LC polymer.[48−54]

Finally, ChEO10 was cooled from 160 °C to a crystallization temperature (T_c = −14 °C) with two thermal histories: (1) cooling at a constant rate of 100 °C/min; (2) first cooling to 20 °C at a rate of 10 °C/min, held at 20 °C for 5 min to form perfect LC phase, and finally cooled to −14 °C. Figure 14 shows the Avrami plots for two crystallization conditions. When the LC phase is preexisting, the Avrami exponent is smaller. This indicates that a preexisting LC phase might have a weak confinement effect on the crystallization of POE and the dimension of crystal growth of POE is reduced, whereas it gives a larger crystallization rate constant (k), which is consistent with the above nonisothermal crystallization result.

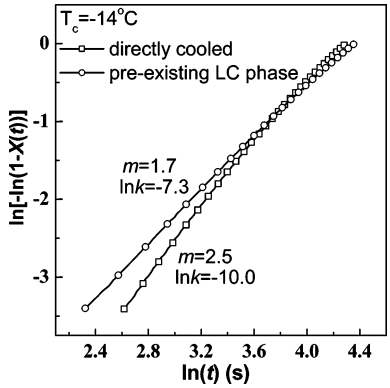

Figure 14. Avrami plots for ChEO10 crystallized at −14 °C after cooling from 160 °C with two cooling histories: (□) represents constant cooling at a rate of 100 °C/min, and (○) represents cooling to 20 °C at a rate of 10 °C/min, then held for 5 min, and finally cooling to −14 °C at a rate of 100 °C/min.

Conclusion

We have shown via DSC, WAXD, Raman spectra, POM, and SAXS that the crystallization of POE moiety becomes the dominant factor in determining the final morphology of ChEO*n*. The coexistence of crystalline POE phase and LC phases was found for ChEO10 and ChEO15. With increasing *n*, LC moieties pack more closely so that the two LC layers merge into one LC layer in the lamellar structure. The preexisting LC phase leads to higher crystallization temperature and faster crystallization rate of the POE moiety, showing that the LC phase can nucleate and accelerate the crystallization of POE moiety. However, the Avrami exponent was reduced, indicating that crystallization of POE moiety is slightly confined by the preexisting LC phase.

Acknowledgment. This project was supported by National Natural Science Foundation of China (20374046), the Excellent Young Teachers Program and New Century Supporting Program for the Talents by Ministry of Education, China. J. K. Kim acknowledges the support of the National Creativity Research Initiative Program supported by the Korea Science and Engineering Foundation.

Supporting Information Available: GPC chromatograms and NMR spectra of all ChEO*n*s, 2D SAXS images of ChEO10 and ChEO15, and the length and width of one cholesterol molecule obtained from the software of "ChemOffice". This material is available free of charge via the Internet at http://pubs.acs.org.

References and Notes

(1) Jiang, M.; Duan, H. W.; Chen, D. Y. *Macromol. Symp.* **2003**, *195*, 165.
(2) Tschierske, C. *Curr. Opin. Colloid Interface Sci.* **2002**, *7*, 355.
(3) Di Marzio, E. A. *Prog. Polym. Sci.* **1999**, *24*, 329.
(4) Forster, S.; Plantenberg, T. *Angew. Chem., Int. Ed.* **2002**, *41*, 689.
(5) Elemans, J.; Rowan, A. E.; Nolte, R. J. M. *J. Mater. Chem.* **2003**, *13*, 2661.

(6) Cornelissen, J.; Fischer, M.; Sommerdijk, N.; Nolte, R. J. M. *Science* **1998**, *280*, 1427.
(7) Kato, T. *Science* **2002**, *295*, 2414.
(8) Ikkala, O.; ten Brinke, G. *Science* **2002**, *295*, 2407.
(9) Thunemann, A. F.; Kubowicz, S.; Burger, C.; Watson, M. D.; Tchebotareva, N.; Mullen, K. *J. Am. Chem. Soc.* **2003**, *125*, 352.
(10) Floudas, G.; Papadopoulos, P.; Klok, H. A.; Vandermeulen, G. W. M.; Rodriguez-Hernandez, J. *Macromolecules* **2003**, *36*, 3673.
(11) Ikkala, O.; ten Brinke, G. *Chem. Commun.* **2004**, 2131.
(12) Wang, X. Z.; Chen, Y. Q.; Chen, X. Z.; Jiang, X. K.; Li, Z. T. *Prog. Chem.* **2005**, *17*, 451.
(13) Chen, J. T.; Thomas, E. L.; Ober, C. K.; Hwang, S. S. *Macromolecules* **1995**, *28*, 1688.
(14) Sanger, J.; Gronski, W.; Maas, S.; Stuhn, B.; Heck, B. *Macromolecules* **1997**, *30*, 6783.
(15) Loo, Y. L.; Register, R. A.; Ryan, A. J. *Macromolecules* **2002**, *35*, 2365.
(16) Chen, Y. Y.; Baker, G. L.; Ding, Y. Q.; Rabolt, J. F. *J. Am. Chem. Soc.* **1999**, *121*, 6962.
(17) Zhu, L.; Cheng, S. Z. D.; Calhoun, B. H.; Ge, Q.; Quirk, R. P.; Thomas, E. L.; Hsiao, B. S.; Yeh, F. J.; Lotz, B. *J. Am. Chem. Soc.* **2000**, *122*, 5957.
(18) Park, C.; Yoon, J.; Thomas, E. L. *Polymer* **2003**, *44*, 6725.
(19) Camerel, F.; Faul, C. F. J. *Chem. Commun.* **2003**, 1958.
(20) Hofmeier, H.; Schubert, U. S. *Chem. Commun.* **2005**, 2423.
(21) Venkataramanan, B.; Ning, Z.; Vittal, J. J.; Valiyaveettil, S. *Crystengcomm* **2005**, *7*, 108.
(22) Fischer, H.; Poser, S.; Arnold, M. *Liq. Cryst.* **1995**, *18*, 503.
(23) Ruokolainen, J.; Saariaho, M.; Ikkala, O.; ten Brinke, G.; Thomas, E. L.; Torkkeli, M.; Serimaa, R. *Macromolecules* **1999**, *32*, 1152.
(24) Schneider, A.; Zanna, J. J.; Yamada, M.; Finkelmann, H.; Thomann, R. *Macromolecules* **2000**, *33*, 649.
(25) Abeysekera, R.; Bushby, R. J.; Caillet, C.; Hamley, I. W.; Lozman, O. R.; Lu, Z. B.; Robards, A. W. *Macromolecules* **2003**, *36*, 1526.
(26) Ansari, I. A.; Castelletto, V.; Mykhaylyk, T.; Hamley, I. W.; Lu, Z. B.; Itoh, T.; Imrie, C. T. *Macromolecules* **2003**, *36*, 8898.
(27) Minich, E. A.; Nowak, A. P.; Deming, T. J.; Pochan, D. J. *Polymer* **2004**, *45*, 1951.
(28) Itoh, T.; Tomikawa, N.; Yamada, M.; Tokita, M.; Hirao, A.; Watanabe, J. *Polym. J.* **2001**, *33*, 783.
(29) Yi, Y.; Fan, X. H.; Wan, X. H.; Li, L.; Zhao, N.; Chen, X. F.; Xu, J.; Zhou, Q. F. *Macromolecules* **2004**, *37*, 7610.
(30) Li, C. Y.; Tenneti, K. K.; Zhang, D.; Zhang, H. L.; Wan, X. H.; Chen, E. Q.; Zhou, Q. F.; Carlos, A. O.; Igos, S.; Hsiao, B. S. *Macromolecules* **2004**, *37*, 2854.
(31) Loo, Y. L.; Register, R. A.; Ryan, A. J.; Dee, G. T. *Macromolecules* **2001**, *34*, 8968.
(32) Xu, J. T.; Turner, S. C.; Fairclough, J. P. A.; Mai, S. M.; Ryan, A. J.; Chaibundit, C.; Booth, C. *Macromolecules* **2002**, *35*, 3614.
(33) Xu, J. T.; Fairclough, J. P. A.; Mai, S. M.; Ryan, A. J.; Chaibundit, C. *Macromolecules* **2002**, *35*, 6937.
(34) Folmer, B. M.; Svensson, M.; Holmberg, K.; Brown, W. *J. Colloid Interface Sci.* **1999**, *213*, 112.
(35) Rodriguez, C.; Naito, N.; Kunieda, H. *Colloids Surf., A* **2001**, *181*, 237.
(36) Sato, T.; Hossain, M. K.; Acharya, D. P.; Glatter, O.; Chiba, A.; Kunieda, H. *J. Phys. Chem. B* **2004**, *108*, 12927.
(37) Lopez-Quintela, M. A.; Akahane, A.; Rodriguez, C.; Kunieda, H. *J. Colloid Interface Sci.* **2002**, *247*, 186.
(38) Avrami, M. *J. Chem. Phys.* **1939**, *7*, 1103.
(39) Dong, B. Z.; Sheng, W. J.; Yang, H. L.; Zhang, Z. J. *J. Appl. Crystallogr.* **1997**, *30*, 877.
(40) Privalko, V. P.; Lobodina, A. P. *Eur. Polym. J.* **1974**, *10*, 1033.
(41) Ding, Y. Q.; Rabolt, J. F.; Chen, Y.; Olson, K. L.; Baker, G. L. *Macromolecules* **2002**, *35*, 3914.
(42) Miao, J. J.; Xu, G. Q.; Zhu, L.; Tian, L.; Uhrich, K. E.; Avila-Orta, C. A.; Hsiao, B. S.; Utz, M. *Macromolecules* **2005**, *38*, 7074.
(43) Yang, Y. W.; Tanodekaew, S.; Mai, S. M.; Booth, C.; Ryan, A. J.; Bras, W.; Viras, K. *Macromolecules* **1995**, *28*, 6029.
(44) Rosch, M. In *Nonionic Surfactants*; Schick, M. J., Ed.; Dekker: New York, 1967; p 753.
(45) Craven, J. R.; Zhang, H.; Booth, C. *J. Chem. Soc., Faraday Trans.* **1991**, *87*, 1183.
(46) Loomis, C.; Shipley, G.; Small, D. *J. Lipid Res.* **1979**, *20*, 525.
(47) Mark, J. E. *Polymer Data Handbook;* Oxford University Press: Oxford, 1999.
(48) Minkova, L. I.; Magagnini, P. L. *Colloid Polym. Sci.* **1996**, *274*, 34.
(49) Gopakumar, T. G.; Ghadage, R. S.; Ponrathnam, S.; Rajan, C. R.; Fradet, A. *Polymer* **1997**, *38*, 2209.
(50) Torre, F. J.; Cortazar, M. M.; Gomez, M. A.; Ellis, G.; Marco, C. *Polymer* **2003**, *44*, 5209.
(51) Kalkar, A. K.; Deshpande, A. A. *Polym. Eng. Sci.* **2001**, *41*, 1597.
(52) Miteva, T.; Minkova, L. *Macromol. Chem. Phys.* **1998**, *199*, 597.
(53) Minkova, L.; Magagnini, P. L. *Polymer* **2001**, *42*, 5607.
(54) Kim, J. Y.; Kang, S. W.; Kim, S. H.; Kim, B. C.; Shim, K. B.; Lee, J. G. *Macromol. Res.* **2005**, *13*, 19.

MA052051S